Astron. Astrophys. 318, 908–924 (1997)

ASTRONOMY AND ASTROPHYSICS

The expansion of the envelope of Nova V 1974 Cygni and the distance problem

D. Chochol[1], **J. Grygar**[2], **T. Pribulla**[1], **R. Komžík**[1], **L. Hric**[1], **and V. Elkin**[3]

[1] Astronomical Institute, Slovak Academy of Sciences, 059 60 Tatranská Lomnica, The Slovak Republic
(Internet: chochol@ta3.sk, pribula@ta3.sk, rkomzik@ta3sk, hric@ta3.sk)
[2] Institute of Physics, The Academy of Sciences of the Czech Republic, Na Slovance 2, 180 40 Praha 8, The Czech Republic
(Internet: grygar@fzu.cz)
[3] Special Astrophysical Observatory, Nizhnij Arkhyz 357147, Karachaevo-Cherkesia, Russia (Internet: vgelk@sao.stavropol.su)

Received 22 September 1994 / Accepted 3 June 1996

Abstract. Available optical and UV spectroscopic, HST and radio imaging observations of the Nova V 1974 Cygni were used to derive a kinematic model of the expansion of the nova shell. The nova shell consists of two major components: an outer fast tenuous low-mass envelope and an inner slow main high-mass envelope. The outer envelope, detected spectroscopically and on radio images, is spherical except for the polar region, where an outflow with twice as large a velocity is observed. The envelope is accelerated by the nova wind that consists of spherical and polar components, too. The most pronounced features of the inner envelope, detected spectroscopically and on the HST images, are an expanding dense equatorial ring and polar blobs. The ring is immersed in the expanding spherical lower density envelope. These structures are accelerated by the wind, too. The polar direction of the outer envelope coincides with the direction of expansion of the ejected blobs of the inner envelope. The HST images taken 818 days after the outburst show clearly the effect of the strong large-scale magnetic field, caused by the interplay of the dipole magnetic field of the white dwarf and the magnetized plasma, on the expanding prolate inner envelope. The "light charged particles" of the outflowing plasma in the polar region follow the magnetic field lines of force in about 10 meridional arcs (flux tubes), which resemble a water fountain. The particles moving in arcs interact with the expanding spherical inner envelope creating visible bright spots. HST images taken between days 467 and 818 show subsequent advance of the equatorial ring. Radial velocities of the components of the inner and outer envelopes and wind were derived from optical and UV spectroscopy. Expansion rates of the components of both envelopes in the plane of the sky were derived from HST images and radio images, respectively. These data were used to determine the inclination of the polar ejecta with respect to the observer. The resulting value of $i = 38\overset{\circ}{.}7 \pm 2\overset{\circ}{.}1$ enabled us to determine the true expansion velocities. Using this kinematic model we were able to review all published distances of the nova. The final value $d = (1.77 \pm 0.11)$ kpc gives a good fit to all available data. It is shown that the white dwarf in Nova V 1974 Cyg is strongly magnetic.

Key words: stars: novae, cataclysmic variables – stars: individual: Nova V 1974 Cygni – stars: distances – stars: circumstellar matter

Send offprint requests to: D. Chochol

1. Introduction

Nova V 1974 Cygni (= Nova Cygni 1992) was discovered by Collins (1992) on February 19, 1992 – the day of the outburst. It reached visual maximum V = 4.4 on February 22 – the day of maximum. It is the brightest nova in the northern hemisphere since 1975 and due to favourable circumstances it is the best-studied nova in the history of astronomy.

It is not the purpose of the paper to review all work done in connection with the outburst of this most interesting nova. Instead, we shall concentrate on a rediscussion of the kinematics of the expanding envelopes of the nova in view of the unique situation provided by the early imaging of the nova envelope with the HST FOC camera. Paresce (1994) determined the distance of the nova in a rather straightforward way, using the angular radius of the nebular envelope and the velocity of its expansion as deduced from early IUE spectra (1500 km s^{-1}). The distance derived by him $d = (3.2 \pm 0.5)$ kpc is surprisingly large and at variance with most of the distance estimations that employed conventional indirect methods. Paresce et al. (1995) extended the range of possible distances from 1.8 to 3.2 kpc assuming the emitting material is expanding at 830 - 1500 km s^{-1}. Thus here we also attempt to clarify the cause of the uncertainty.

Table 1. Review of the colour excesses and distance estimations from absolute magnitudes at maximum light of Nova V 1974 Cyg

Reference	t_2	t_3	$M_V^{(max)}$	$M_B^{(max)}$	E(B–V)	distance [kpc]	Method
Andrillat & Houziaux (1993)		55		-7.53	0.37	2	M_B –t_3 relation
Annuk et al. (1993)	16	40	-7.74	-7.79	0.42	1.3	M_V –t_3 relation
Anupama & Prabhu (1993)					0.31	1.6	M_V –$t_{2,3}$ relations
Austin et al. (1993)	24				0.3 ± 0.1	1.7 ± 0.2	M_V –t_3 relation
Chochol et al. (1993)	16	42	-7.67		0.32 ± 0.01	1.77 ± 0.11	$M_{V,B} - t_{2,3}$ relations
	23	51		-7.49			V_{15}, B_{15} relations
DellaValle & Livio (1995)	16		-8.3		0.0 - 0.32	2.2 – 3.4	M_V –t_2 relation
Elias et al. (1992)			-7.7			1.3 – 2.5	
Hayward et al. (1992)	17		-7.55		0.34	2.1	M_V –t_2 relation
Kolotilov et al. (1994)	25	47	-7.3		0.25	1.35	M_V –t_3, V_{15} relations
Pavelin et al. (1993)			-7.7		0.3	1.8 ± 0.4	V_{15} relation
Rafanelli et al. (1995)	16		-8.3		0.17	2.8	M_V –t_2 relation (Capaccioli et al., 1989)
Shara (1994)		47		-7.6	0.0	2.8	M_B –t_3 relation
Shore (1992)					0.35 ± 0.05	1.5 ± 0.5	
Shore et al. (1992)					0.2 – 0.4	1 – 2	$M_{bol}^{(max)} = M_{Edd}(1M_\odot)$
Shore et al. (1994)					0.2 ± 0.05; 0.25	3	$M_{bol}^{(max)} = M_{bol}$ for Nova LMC 1990 No.1
Mean values			**-7.78 ± 0.12**	**-7.60 ± 0.06**	**0.26 ± 0.03**	**2.0 ± 0.2**	
Mean value of distance excluding the values larger than 2.7 kpc						**1.72 ± 0.1**	

2. Review of distance determinations of V 1974 Cygni

In our previous paper (Chochol et al., 1993) we tried to determine the distance of the nova by measuring the equivalent widths of the Ca II H and K interstellar lines. This procedure led to an unplausibly low value of $d = 0.6$ kpc. Similarly, Annuk et al. (1993) using the same method obtained the distance of $d = (1.4 \pm 0.1)$ kpc. The obvious disadvantage of this procedure is its sensitivity to contamination by the circumstellar lines of Ca II and H I. Thus we prefer to reject the data as unreliable.

The most widespread distance determination method for novae is based on the estimate of absolute magnitude at maximum light (e.g. by the MMRD - relation) and on the evaluation of interstellar extinction. Both parameters are, of course, sensitive to various sources of errors. However, there are several well established techniques to estimate these errors and therefore proper analysis may lead to reliable determination of the nova distance.

Most authors estimated the absolute magnitude of the nova in maximum by employing various statistical relations between absolute magnitude in a given colour of a broadband colour system and the time of the decay of the light curve by two (t_2) or three (t_3) magnitudes below maximum light. A review of published data is given in Table 1.

As it is easily seen from Table 1, the values of absolute magnitude and distance of Nova V 1974 Cyg published by various authors are in reasonable mutual agreement. There are, however, exceptions, namely the results of Shore et al. (1994), Rafanelli et al. (1995) and Della Valle & Livio (1995). They all derived the absolute magnitude using the evidence for novae in near neighbour galaxies (LMC; M 31). Della Valle & Livio (1995) derived an absolutely calibrated MMRD relation:

$$MV_{max} = -7.92 - 0.81 \arctan \frac{1.32 - \log t_2}{0.23} \quad (1)$$

and calculated the absolute magnitude of Nova V 1974 Cyg at maximum as MV_{max} = -8.3. The relation can undoubtedly serve as the best tool for the estimation of the absolute magnitudes of novae at maximum. However, the weak point of the relation is that it connects absolute visual magnitude with the rate of decline in V colour (v_d = 0.125 mag/day) for the decay time t_2 only. It is easy to calculate using the data in Table 1, that the daily rate of decline (given by $t_2/2$ and $t_3/3$) significantly depends on decay times as well as on the colour. The daily rate of decline calculated from $t_{3,V}$ time is v_d = 0.071 mag/day. If we wish to employ the more reliable t_3 time (instead of t_2 time) in relation (1), we have to transform t_3 to t_2 time. Capacciolli et al. (1990) published the following transformation formula. If $t_3 < 80$ days (this is certainly true for Nova V 1974 Cygni), then

$$t_3 = (1.68 \pm 0.08)\, t_2 + (1.9 \pm 1.5)\, days. \quad (2)$$

By applying this relation we easily find $t_{2,Vtransf} = (23.9 \pm 2.1)$ days. The corresponding MV_{max} = (-7.72 ± 0.13) is then in full agreement with other calculations of MV_{max}.

The low extinction coefficients in the direction of Nova V 1974 Cyg were determined rather artificially - we believe that

Table 2. Angular radius of the nova envelope and related distance of the nova

Reference	Day after outburst	Angular radius	Daily rate of expansion	Adopted vel. of expansion [km s^{-1}]	Distance [kpc]	Method
Quirrenbach et al. (1993)	10	$0''.002535$	$2''.53\,10^{-4}$	1000 – 1300	2.3 – 2.9	oi
Hjellming (1994)	313	$0''.175$	$5''.591\,10^{-4}$	1940	2.0	ri,*
	313	$0''.08$	$2''.555\,10^{-4}$	890	2.0	ri,**
Paresce (1994)	467	$0''.13 \pm 0''.022$	$2''.78\,10^{-4}$	1500 ± 250	3.2 ± 0.5	di
Paresce et al. (1995)	467 - 818		$2''.97\,10^{-4}$	830 – 1500	1.8 – 3.2	di

oi – optical interferometry; **ri** – radio interferometry(* outer; ** inner edge of the shell); **di** – direct imaging

Table 3. The journal of spectroscopic observations

JD date	Date	Day	Time UT	t_{exp} min.
49641.315	1994 Oct 15	970	19:34	30
49641.347	1994 Oct 15	970	20:20	30
49642.212	1994 Oct 16	971	17:05	30
49642.235	1994 Oct 16	971	17:38	30
49642.354	1994 Oct 16	971	20:30	30
49877.517	1995 Jun 9	1206	0:24	30

Table 4. The journal of IUE observations

SWP spectrum	JD date	Date 1992+		Time UT	t_{exp} min.
44633	48752.3681	May	9	20:50	40
44718	48761.7486	May	19	5:58	40
44763	48767.7424	May	25	5:49	40
44791	48770.3708	May	27	20:54	40
44792	48770.4194	May	27	22:04	40
44809	48772.7125	May	30	5:06	40
44810	48772.7687	May	30	6:27	40
44902	48783.3472	Jun	9	20:20	65
44971	48795.4882	Jun	21	23:43	40
44972	48795.5681	Jun	22	1:38	100
45031	48802.6354	Jun	29	3:15	40
45032	48802.6903	Jun	29	4:34	30
45060	48807.2556	Jul	3	18:08	83
45062	48807.3951	Jul	3	21:29	45
45136	48818.2451	Jul	14	17:53	110
45245	48833.1965	Jul	29	16:43	93
45360	48851.5187	Aug	17	0:27	42
45468	48864.3069	Aug	29	19:22	90
45470	48864.4854	Aug	29	23:39	136
45549	48873.0875	Sep	7	14:06	85

the authors were a priori influenced by the distance determination of the nova from the first HST imaging (see Paresce, 1994). Nova V 1974 Cyg is located near the galactic plane (b = $7^\circ.8$); so the assumption of $A_V = 0$ introduced by Shara (1994) and accepted by Della Valle & Livio (1995) is quite absurd. Mathis et al. (1995) critically evaluated the reddenings published by different authors and concluded that the possible absorptions are within the interval 0.59 - 1.0 (reddenings E(B-V) being between 0.19 and 0.32). As was pointed out by Paresce et al. (1995), the spectrum of the nova shows a prominent broad absorption feature centered at 220 nm caused by the interstellar extinction. They removed the feature assuming a value for E(B-V) = 0.35.

Although the accurate determination of the interstellar extinction as well as of the absolute magnitudes of novae is difficult, we conclude that the true distance of the nova can hardly be larger than 2.2 kpc unless one assumes unrealistically low interstellar extinction in the given direction and/or an extremely bright absolute magnitude of the nova.

However, advances in observational techniques gave us the opportunity of true distance determination based on nebular expansion parallaxes. When the angular diameter (and shape) of the expanding envelope is resolved and if we knew the true projected expansion velocity of the envelope from high-dispersion spectra, the determination of the distance of the nova is almost trivial.

In the meantime several measurements of the diameter of the nova envelope have been published and the distance of the nova was determined under specific (sometimes possibly poor) values for the average expansion velocity (see Table 2.)

Contrary to expectations, the spread of distances is large and the a priori most reliable distance determination through the optical imaging of the envelope by the FOC camera of the HST lies well above the limit set by previous indirect methods. As noted by Paresce (1994), the possible weakness of the geometric method lies in the uncertain selection of the "proper" expansion velocity from the early spectra of the nova. We believe that this is a crucial problem, affecting profoundly the distance determination in all similar cases, for novae and possibly also for supernova remnants.

It is well-known from the classical work of McLaughlin (1943) that the velocity development in the spectra after outburst is complex, and several systems with widely different velocities develop in the course of time. The ratio of different velocities easily exceeds 2:1, and thus it is not easy to predict correctly which velocity values correspond to the observed angular size

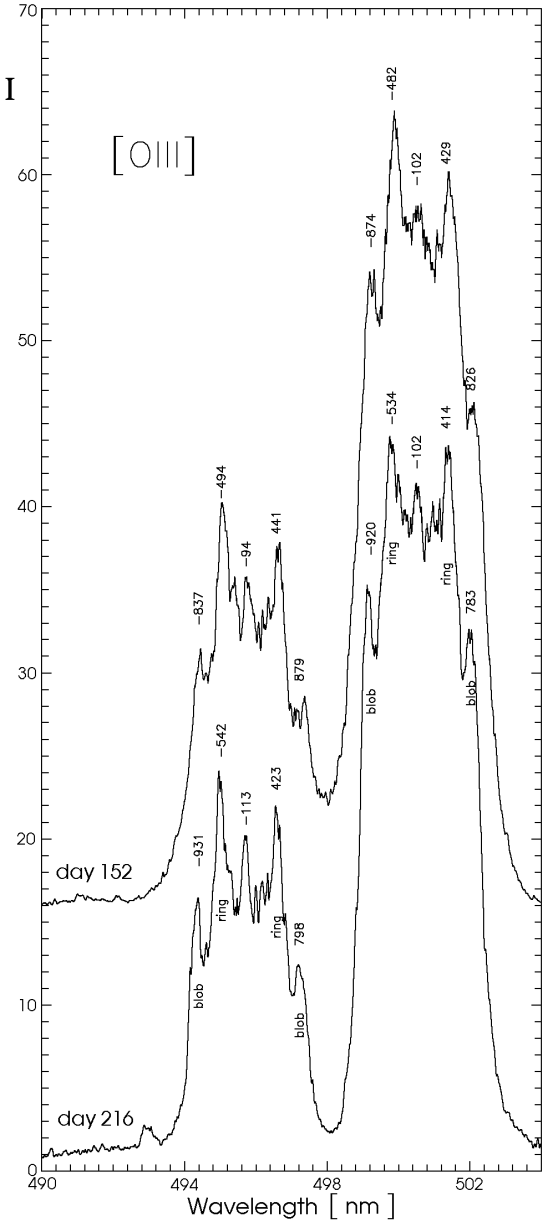

Fig. 1. [O III] emission lines profiles of Nova V 1974 Cyg on July 20, 1992 (day 152 after outburst) and September 22, 1992 (day 216 after outburst)

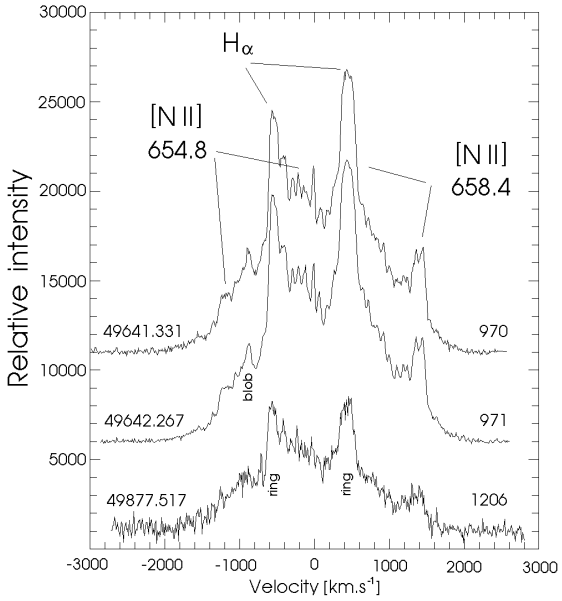

Fig. 2. H_α emission line profiles

3. Spectroscopic observations and data reduction

3.1. Optical spectra

Chochol et al. (1993) found in the high resolution tracings of the H_β line in the nebular stage of Nova V 1974 Cyg, taken on days 152 and 216 after the outburst, a splitting of the line profile into a few components corresponding to approaching and receding parts of an expanding equatorial ring and two polar blobs. In Fig. 1 we reproduce the emission profiles of [O III] lines taken on July 20 and Sept. 22, 1992 (152 and 216 days after outburst). They reveal the same behaviour. Detailed description of our spectroscopic observations was published by Chochol et al. (1993).

We obtained further optical spectra using the CCD camera and main stellar spectrograph of the 6 m telescope of the SAO at Nizhnij Arkhyz in Russia. Spectrograms with dispersion 1.4 nm mm^{-1} covered the H_α spectral region. The spectral resolution was 0.07 nm. The journal of observations is given in Table 3. The spectra are depicted in Fig. 2. Resulting profiles on days 970 and 971 were obtained by summing up two and three spectra, respectively.

3.2. UV IUE spectra

Shore et al. (1993) published the evolution of the high resolution UV line profiles of Nova V 1974 Cyg from day 2 to 409 after the outburst using the IUE and HST GHRS spectra. To explain the complicated emission line profiles with many filaments during the nebular stage, they supposed a random spherical distribution of the emitting material around the central source. They simulated the structure of emission line profiles using a Monte Carlo method.

of the nova envelope. Moreover, there is ample evidence that the velocities of given segments of the envelope change with time due to the changes of driving force and/or the interaction of the envelope with the circumstellar medium.

Wade (1990) found that most of 26 resolved nebular remnants of classical novae are prolate in outline, with substructures that can be characterized as consisting of polar blobs and equatorial rings. Boyarchuk and Gershberg (1977) found these substructures spectroscopically in the expanding envelope of Nova V 1500 Cyg.

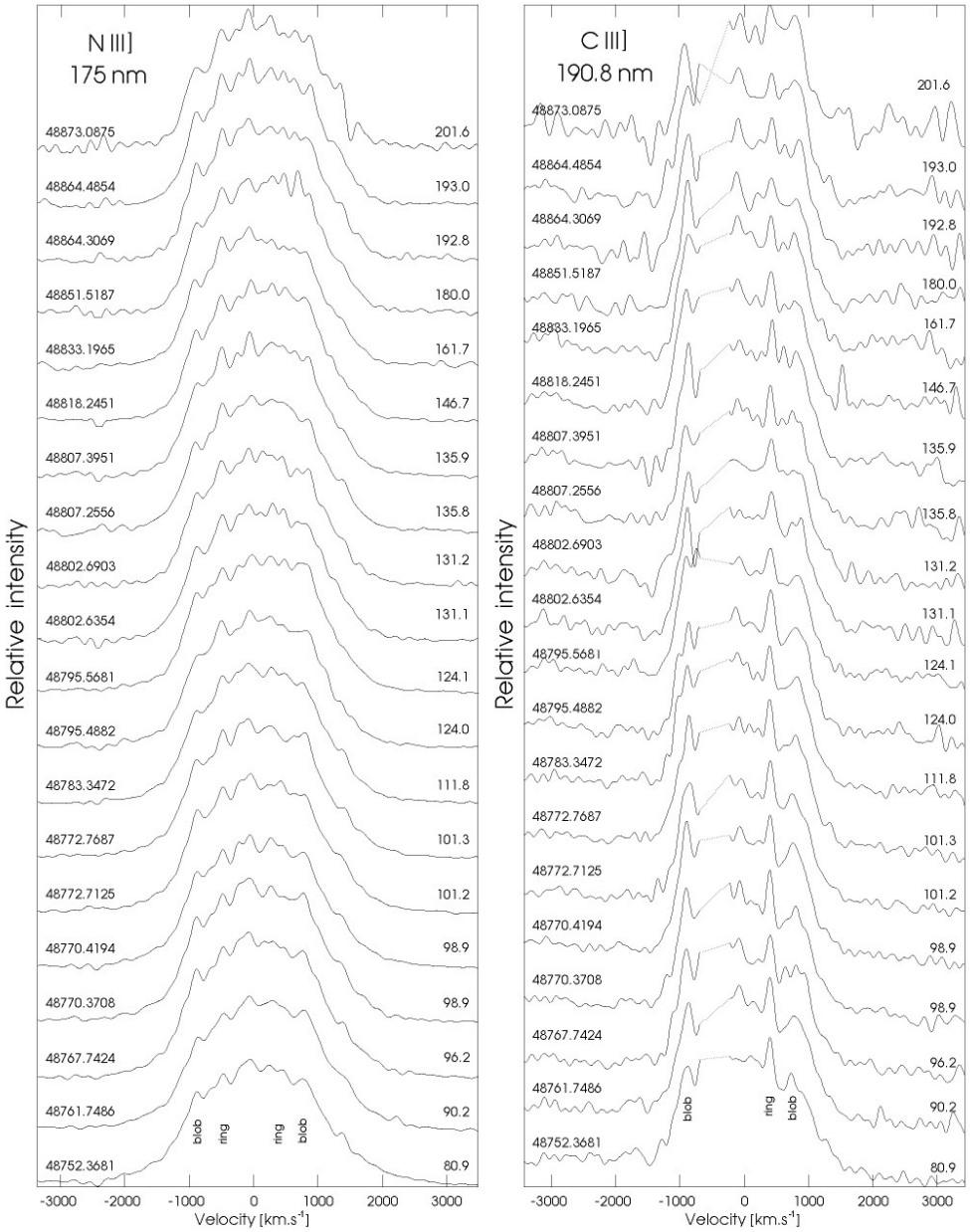

Fig. 3. N III] and C III] line profiles

In the present paper we reanalyze IUE SWP spectra in the nebular stage of Nova V 1974 Cyg from day 80 to 202. The spectra were extracted from the IUE archive at Villafranca and further processing was done using standard ESO MIDAS software and the SPEFO code written by Horn (1992). The journal of observations is given in Table 4.

Fig. 3 displays an evolution in the UV line profiles of N III] 175 nm and C III] 190.8 nm lines. The spectra were normalized to the maximum of the line intensity and filtered by a filter of 0.06 nm width. As in the optical spectra, the emission peaks, belonging to the expanding ring and blobs, are clearly visible and their radial velocities are very stable. Other UV lines are either very weak or blended, so they are not suitable for measurements of the radial velocities of emission peaks. The emission peak of the C III] line belonging to the approaching expanding ring is located exactly in the spectral region where different echelle orders of the spectrum overlap each other. As the line intensity in this region is very uncertain we removed this part of the line profile and designated it by the dashed line.

It is clear that the emission peaks are stable over several months and represent well the principal components of the expanding envelope, namely the very thin equatorial ring plus two polar blobs (visible also in the HST images). The central emission peak is caused by the movement of gaseous structures in the plane perpendicular to the line of sight.

4. HST images of the expanding envelope

The detailed description of the HST images of the expanding envelope taken on days 467, 689, 726 and 818 as well as data

reduction procedures were published by Paresce et al. (1995). The main feature is the bright elliptical ring best visible in H_β and [O III] lines, which linearly expands along the semi-major axis by 0.297 mas/day and along the semi-minor axis (defined by two bright knots) by 0.218 mas/day. According to Paresce et al. (1995) the major axis of the bright ring defines polar direction!

In our rediscussion we used the images given in Table 5. All the images were treated using the standard procedures described by Nota et al. (1994) as well as using the point spread functions derived from observations of bright single stars through the same filters. The standard IRAF and MIDAS packages were used for further processing. The images from the same observing run, where the bright ring was well defined, were merged. Since the ring was not uniform in brightness, we chose 3 tresholds corresponding to different intensities. The central part of the image was removed. It is apparent that the ring in all cases was well defined by an ellipse.

In our interpretation the bright ring is identical with the circular equatorial ring. In this case the elliptical shape of the ring is caused by the projection of the circular ring onto the celestial sphere. An inclination angle i of the equatorial ring plane against the celestial sphere can be calculated as follows: The radius vector of the point of the ring r at azimuth angle A is given by:

$$r = r_{\max} \cos i \sqrt{\frac{1 + \tan^2 (A - \Omega)}{\cos^2 i + \tan^2 (A - \Omega)}}, \qquad (3)$$

where $r_{\max}$ is the true radius of the ring (equal to semimajor axis of the ellipse) and Ω is the azimuth angle of the ascending node measured from the north point of the ring eastward. Fitting of the isophotes by a general least square method using the simplex downhill method and Eq. (3) for the best coordinates of the ring centre, we obtained i and Ω as given in Fig. 4. We also measured the projected angular distances of the blobs from the center of the nebula. Using these values we constructed the diagram on Fig. 7 formally similar to Fig. 6 in the paper by Paresce et al. (1995). However, by the inspection of Fig. 4 we see that the minor axis is not defined by two bright knots as supposed by Paresce et al. (1995). These knots designated by crosses are in fact the polar blobs and move independently with respect to the ring. Comparison of the images in Fig. 4 also shows that i and Ω of the ring change with time. If we suppose the linear increase of i and decrease of Ω as it is depicted in Figs. 8 and 9, we can easily predict their values during the expansion of the envelope.

The first HST image of Nova V 1974 Cyg taken on day 467, in time before installation of COSTAR, is highly problematic (see Fig. 5). Our processing of the image by the same method as in previous three images led to the value of $\Omega = 67\overset{\circ}{.}5$. If this were true, the orientation of the ring has changed in time for an unbelievably large amount and in an unpredictable way. However, the flipped image gives $\Omega = 112\overset{\circ}{.}5$, in good agreement with the predicted values (see Fig. 8). Therefore we believe that the sign of matrix of the orientation of the image in the header of the pre-COSTAR image is incorrect. A further problem arises with the inclination angle. In the image which we have processed

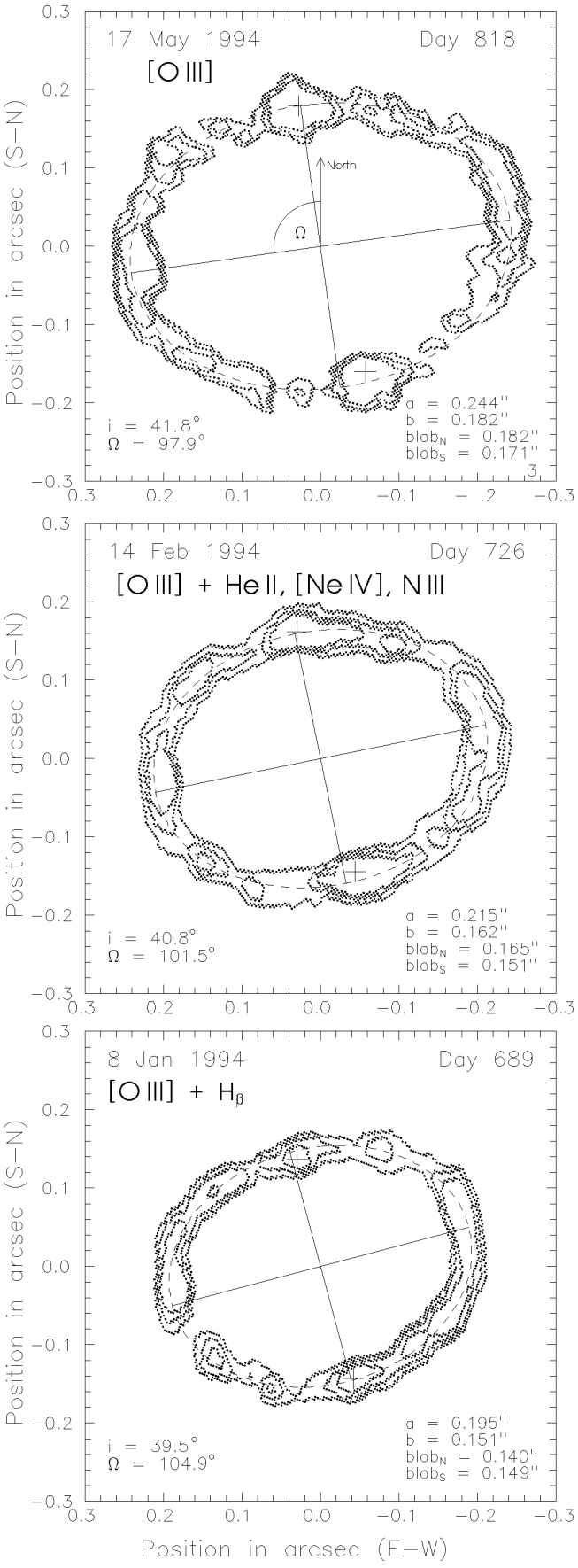

Fig. 4. Parameters of the equatorial ring and polar blobs

Table 5. Journal of HST images

Filter	Date		Day	Format	t_{exp} sec	Spectral line	Comment
F278M	1993 May	31	467	256x256	897	Mg II	Pre-COSTAR
F486N	1994 Jan	8	689	256x256	896	H_β	
F501N	1994 Jan	9	690	256x256	896	[O III]	
F470M+F1ND	1994 Feb	14	726	256x256	896	N III, He II, [Ne IV]	
F501N+F2ND	1994 Feb	14	726	256x256	596	[O III]	
F346M+F3ND	1994 May	17	818	512x512	896	[Ne V]	
F501N+F1ND	1994 May	17	818	512x512	896	[O III]	

only the brightest parts of the ring were taken and the ring was not well defined. Moreover as it is easily seen from Fig. 7, the length of the semi-major axis is underestimated. So the value of $i = 39^\circ.5$ could only be the upper limit of the possible inclination angle of the ring. For the determination of i we used also the image processed in STScI by Paresce (1994) and available in the HST ftp server. We delineated the contour of the ring by identifying the pixels with the same intensity at the edge of the ring and measuring their positions given by radius vector against the azimuth angle. The resulting value is $i = 33^\circ.5$ as it is shown in Fig. 6. The mean value of the inclination angle found by these two methods is $i = 36^\circ.5 \pm 2^\circ.1$. This value is in agreement with the predicted value found by the extrapolation of i from other 3 images in Fig. 9.

Among the available HST images of the expanding envelope of the nova, the last two (May 17, 1994 = day 818) are the most remarkable. Fig. 10 was obtained by superposition of the HST images in [Ne V] and [O III] lines. We interpret it as an evidence for a magnetic force shaping of the inner envelope up to a distance of about 450 AU from the nova caused by the interplay between the dipole magnetic field of the underlying white dwarf and magnetized plasma. The "light particles" of the outflowing plasma in the polar region follow the magnetic lines of force forming about 10 arc-like meridional streams (flux tubes) resembling a water fountain. The points of intersection of these streams with the expanding spherical lower density inner envelope are clearly seen as the bright spots within the shell (Fig. 11). If we suppose that the bright spots are located on a circle, we can calculate the position of the magnetic field axis on day 818 using the same method as in the case of the equatorial ring. The resulting value is $i = 51^\circ.0$. It is clear that the polar axis of the expanding envelope is defined by the symmetry axis of the fountain. This direction is nearly perpendicular to the direction of the major axis of the ring, which according to Paresce et al. (1995) defines the polar direction.

5. Basic equations

5.1. Case of axial symmetry

Radial velocities of the expanding equatorial ring and polar blobs determined spectroscopically and tangential velocities determined from the HST or radio images can be used simultaneously for calculation of the true expansion velocities v of the ring and blobs, as indicated in Fig. 12, using the equations:

$$RV_{\rm blob} = v_{\rm blob}\cos i, RV_{\rm ring} = v_{\rm ring}\sin i \quad (4)$$

$$TV_{\rm blob} = v_{\rm blob}\sin i, TV_{\rm ring}^{\rm max} = v_{\rm ring}. \quad (5)$$

The most important parameter - the inclination angle i - can be calculated, using the equation:

$$\tan i\ sini = \frac{RV_{\rm ring}}{RV_{\rm blob}} \times \frac{TV_{\rm blob}}{TV_{\rm ring}^{\rm max}} \quad (6)$$

The ratio of radial velocities can be found directly from spectroscopic observations. The ratio of tangential velocities is identical to the ratio of expansion rates for the blobs and ring determined in Fig. 7. If the inclination angle i is known, the true velocities of the ring and blobs can be calculated using the Eq. (4).

5.2. Non-axially symmetric case

In this case the inclination angle of the ring i' differs from the inclination angle i of the blobs. The basic equations are modified as follows

$$RV_{\rm blob} = v_{\rm blob}\cos i, RV_{\rm ring} = v_{\rm ring}\sin i' \quad (7)$$

$$TV_{\rm blob} = v_{\rm blob}\sin i, TV_{\rm ring}^{\rm max} = v_{\rm ring} \quad (8)$$

The two inclination angles i and i' are related by the equation:

$$\tan i \sin i' = \frac{RV_{\rm ring}}{RV_{\rm blob}} \times \frac{TV_{\rm blob}}{TV_{\rm ring}^{\rm max}} \quad (9)$$

5.3. Spherical envelope with outflow in polar region

The basic equations are modified as follows:

$$RV_{\rm blob} = v_{\rm blob}\cos i, RV_{\rm sphere} = v_{\rm sphere} \quad (10)$$

$$TV_{\rm blob} = v_{\rm blob}\sin i, TV_{\rm sphere} = v_{\rm sphere} \quad (11)$$

The inclination angle can be calculated using the equation

$$\tan i = \frac{RV_{\rm sphere}}{RV_{\rm blob}} \times \frac{TV_{\rm blob}}{TV_{\rm sphere}} \quad (12)$$

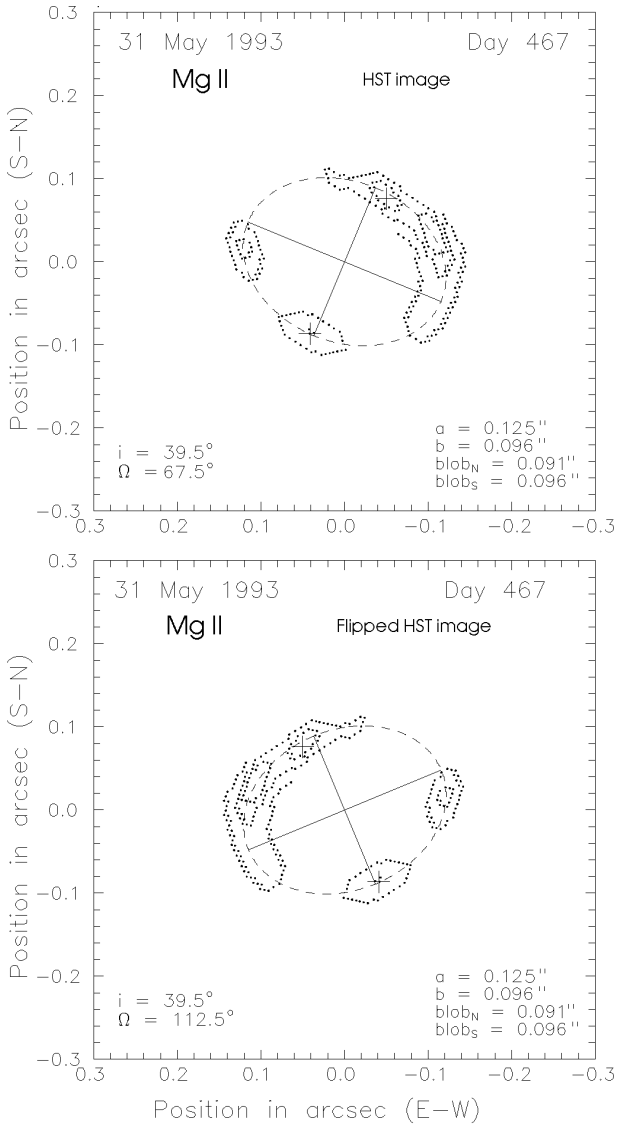

Fig. 5. Parameters of the equatorial ring and polar blobs on day 467

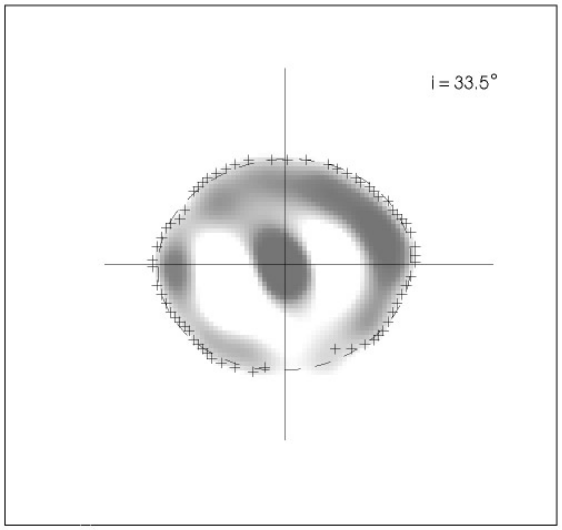

Fig. 6. Determination of the inclination angle from the HST image taken on day 467.

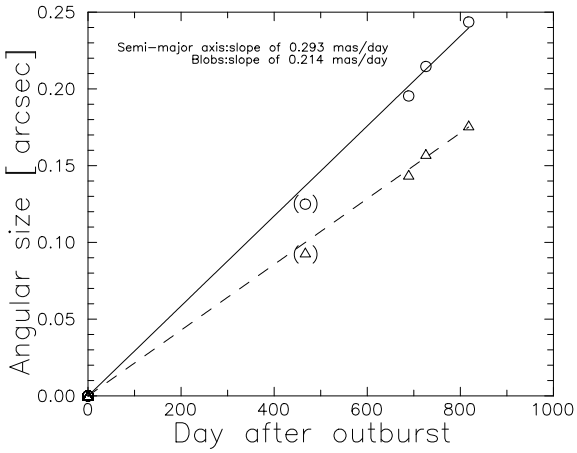

Fig. 7. The expansion rates of the equatorial ring and polar blobs. The values in the brackets were not used for the fits.

6. Kinematic model of the expanding envelope

6.1. Winds from the hot component

During the outburst of nova a mass shell is ejected as a consequence of a thermonuclear runaway on the white dwarf. After the ejection of the shell the mass loss continues in the form of the wind. Several mechanisms provide the energy for the wind. The most important one is the radiation pressure caused by the hot white dwarf.

The wind can be detected spectroscopically as the broad absorption in P Cygni profiles of UV and optical spectral lines. The line profiles of the Mg II lines in early UV spectra (Fig. 2 of the paper of Shore et al. (1993)) indicate the presence of a wind consisting of spherical and polar components. Very broad absorption centered at about 2400 km s^{-1} is caused by the spherical wind (A). The polar wind (B) forms the small absorption at about 4000 km s^{-1}. As it is possible to see from Table 6 and Fig. 13, the RV of the wind absorptions seen in the UV region corresponds to the RV of double absorptions in the Orion spectrum seen in the visual region after day 48 (Chochol et al. 1993). The Orion absorptions are caused by the spherical and polar winds.

6.2. Outer envelope

The visual spectra of Nova V 1974 Cyg taken soon after maximum light showed the lines of superposed P -Cygni type profiles. Two violet-shifted absorption components with a central emission were visible (Chochol et al. 1993). Each can be considered to be produced in a different region of the outer envelope approaching the observer. Regions not approaching the observer contributed to the emission part of the profile. The increasing wavelength shift of double absorptions with time suggests that the outer expanding envelope was accelerated by the wind. Radial velocities of double absorptions are given in Table 7 and

Table 6. Radial velocities of the spherical (A) and polar (B) wind absorptions

Reference	Day after outburst	RV_{windA} [km s^{-1}]	RV_{windB} [km s^{-1}]	RV_{windA}/RV_{windB}	Sp. lines used for RV determination
this paper	48	-2860	-4670	0.612	H_γ – H_δ
	49	-2740	-4420	0.620	H_γ – H_δ
	52	-2690	-4550	0.591	H_γ – H_δ
	62	-2700	-4430	0.609	H_δ
Shore et al. (1993)	2.05	-2400	-3790	0.633	UV: Mg II
and this paper	2.97	-2410	-3960	0.608	UV: Mg II
	3.82	-2330	-3970	0.587	UV: Mg II
	4.96	-2210	-3910	0.565	UV: Mg II
	6.18	-2230	-3980	0.560	UV: Mg II
	7.18	-2310	-4010	0.576	UV: Mg II
	12.99	-2390	-4140	0.577	UV: Mg II
	13.09	-2410	-4260	0.566	UV: Mg II
	14.83	-2450	-4400	0.557	UV: Mg II
	21.98	-2820	-4360	0.647	UV: Mg II
	28.94	-2820	-4530	0.622	UV: Mg II
	29.05	-2780	-4580	0.607	UV: Mg II
	43.81	-3000			UV: Mg II
	51.99	-2970			UV: Mg II
Mean value				**0.596 ± 0.007**	

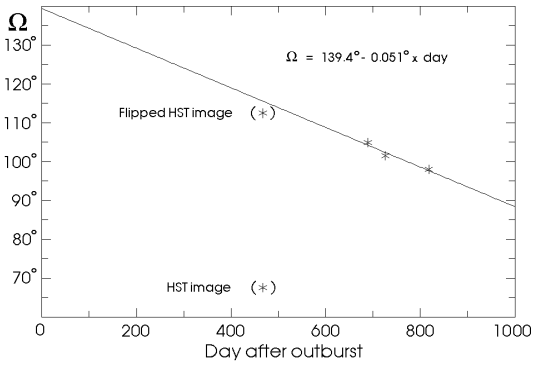

Fig. 8. Time dependence of the position angle of the expanding equatorial ring. The values in the brackets were not used for the fit.

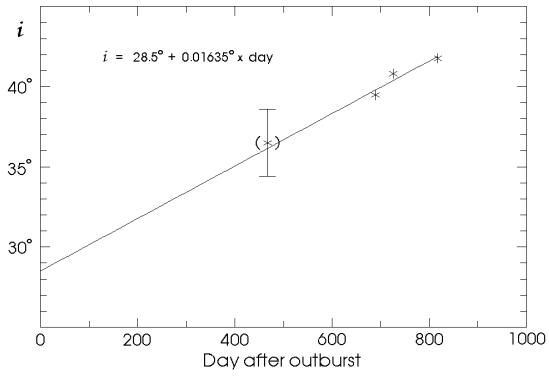

Fig. 9. Time dependence of the inclination of the expanding equatorial ring. The value in the brackets was not used for the fit.

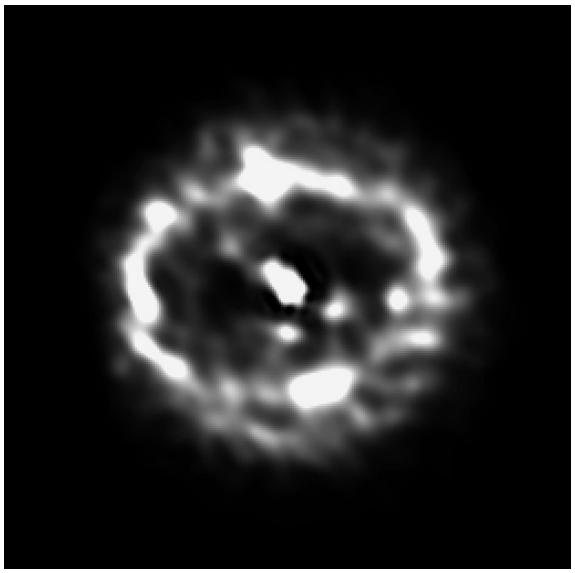

Fig. 10. HST image of the magnetic fountain in the inner envelope

in Fig. 13. As we will show later, in the case of an expanding inner envelope both the approaching and receding RV sets were available, so the data could be used also for the determination of the gamma velocity of the system (see the footnote under the Table 8). Our data represent the radial velocities of the approaching parts of the outer envelope only, so a correction for gamma velocity was necessary. As it is possible to see from Table 6 and Table 7 the ratio of absorptions caused by the components of the wind is the same as in the case of the com-

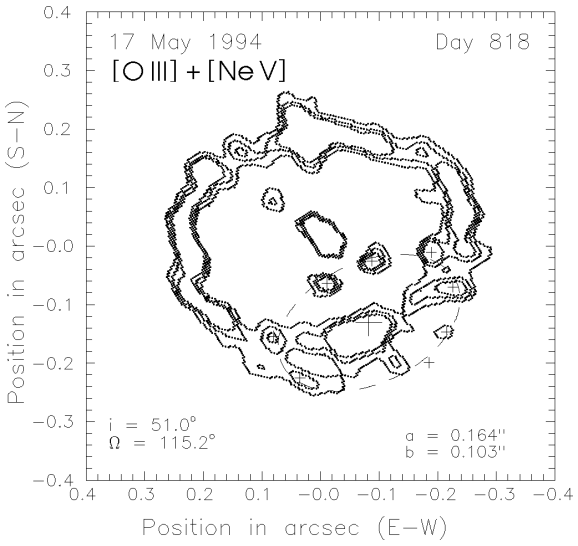

Fig. 11. Magnetic fountain in the inner envelope

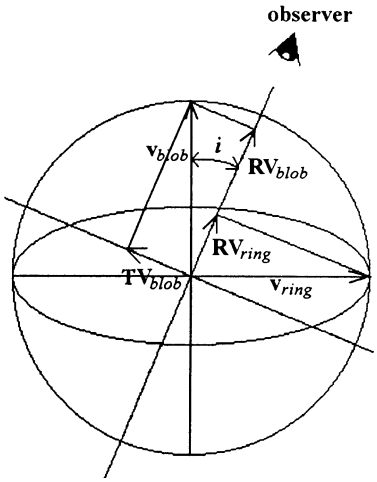

Fig. 12. Radial, tangential and true velocities of the components (blob and ring) of the nova envelope

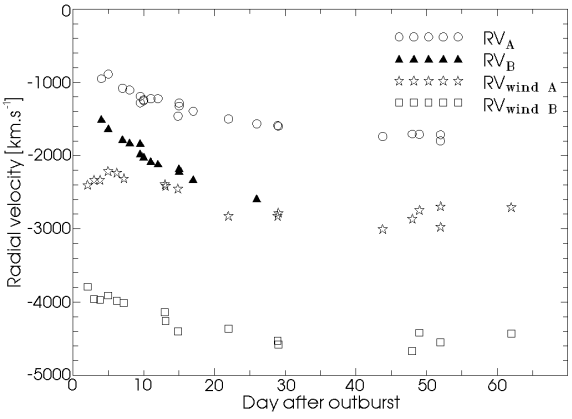

Fig. 13. Radial velocities of the spherical (A) and polar (B) wind, the spherical (A) and polar (B) component of the expanding low-mass outer envelope

ponents of the outer envelope. We can conclude that shaping of the outer envelope was caused by the components of the wind, so it is natural that the outer envelope consisted of the spherical (A) and polar (B) components, too.

The optical spectra taken in early days after outburst (diffuse enhanced spectrum) reflected the expansion of the outer envelope detected as the radio envelope later on. The first two radio images, where the radio envelope was well developed were taken by Eyres et al. (1996) at 6cm by MERLIN on days 154 and 172. The envelope was elliptical indicating a roughly North-South elongation. The angular extent of emission in mas for given brightness temperature in two perpendicular elongations was as follows: day 154: 7500 K (200,160), 10000 K (180,140), 15000 K (150,110), 20000 K (110,80), 30000 K (50,50), day 172: 7500 K (260,190), 10000 K (240,170), 15000 K (210,150), 20000K (190,130), 30000K (160,90), 45000K (100,70). The mean ratio of the major to minor axis (i.e. the ratio of the angular extent of projected polar components to the diameter of the sphere) is $\phi = 1.37 \pm 0.05$. This ratio is the same as the ratio of the major to minor axis of the maximum dimensions of the nova envelope on day 172, which allows to calculate the daily rates of expansion in semi-major and semi-minor axis as 0.7558 mas and 0.5523 mas, respectively. Using the ratio of this rates, which is equal to the ratio of tangential velocities and using the ratio of radial velocities of the same components from Table 7, we calculate the inclination angle of the polar outflow with respect to the observer from relation (12) as $i = 39^\circ 2 \pm 1^\circ 5$.

6.3. Inner main envelope - crude model of expansion

It is well known that the principal spectrum, which appears at visual maximum, reflects the expansion velocity of the main envelope of the nova visible later on as emission lines of nebular spectrum (McLaughlin, 1960; Gallagher and Anderson, 1976). The expansion velocity of the main envelope of Nova V 1974 Cyg, as derived by Andrillat and Houziaux (1993) from principal spectrum, was 800 km s^{-1}. In Fig. 14 we present expansion velocities of the main envelope of the nova measured by us from emission lines taken in nebular stage using the optical spectra (Chochol et al., 1993), the IUE spectra (this paper) and the HST GHRS spectra published by Shore et al. (1993). We measured the full width at half maximum of the emission lines, which is a suitable measure of twice the expansion velocity of the shell (Cohen and Rosenthal, 1983). As it is clearly seen from Fig. 14 the upper limit of expansion velocity of Nova V 1974 Cyg is 1100 km s^{-1}, which is in large disagreement with the value v = 1500 km s^{-1} used by Paresce (1994) for the distance determination. By inspecting Fig. 15, which shows the dependence of the true expansion velocity on t_3 time for many well-observed novae, one may easily infer that Paresce's value is out of the range observed in almost all novae. The data for Fig. 15 were extracted from Slavin et al. (1995). The empirical v - t_3 relation, which we have found from the nebular spectra of 13 novae:

$$\log v = 3.22 - 0.22 \log t_3 \qquad (13)$$

Table 7. Radial velocities of double absorptions in P Cyg profiles caused by the spherical (A) and polar (B) component of the outer envelope

Reference	Day after outburst	RV_A [km s^{-1}]	RV_B [km s^{-1}]	RV_A/RV_B	Sp. lines used for RV determination
Andrillat & Houziaux (1993)	4	-950	-1500	0.623	P_7, P_{12}, P_{14}
	5	-888	-1627	0.534	N I
Baruffolo et al. (1992)	9 – 10	-1190	-1830	0.642	O I
	9 – 10	-1280	-1970	0.642	Balmer H lines
Annuk et al. (1993)	7	-1080	-1777	0.599	Ca II, $H_\beta - H_\epsilon$, Mg II, Fe II
	8	-1106	-1823	0.599	Ca II, $H_\beta - H_\epsilon$, Mg II, Fe II
	12	-1221	-2108	0.571	Ca II, $H_\beta - H_\epsilon$, Mg II
	15	-1282	-2170	0.583	Ca II, $H_\beta - H_\epsilon$, Mg II
	17	-1393	-2324	0.592	Ca II, $H_\beta - H_\epsilon$, Mg II, He I
	26	-1564	-2583	0.599	Ca II, $H_\beta - H_\epsilon$, Mg II, He I
this paper	10	-1250	-2014	0.613	$H_\beta - H_\epsilon$
	10	-1241	-2018	0.607	$H_\beta - H_{10}$
	11	-1222	-2076	0.581	$H_\beta - H_9$
	15	-1324	-2213	0.609	$H_\beta - H_{10}$
	48	-1705			$H_\gamma - H_\delta$
	49	-1711			$H_\gamma - H_\delta$
	52	-1713			$H_\gamma - H_\delta$
Shore et al. (1993)	14.83	-1460			UV: Mg II
	21.98	-1500			UV: Mg II
	28.94	-1590			UV: Mg II
	29.05	-1600			UV: Mg II
	43.81	-1740			UV: Mg II
	51.99	-1800			UV: Mg II
Mean value				**0.596 ± 0.007**	

before the calculation of RV_A/RV_B all RV values were corrected for the γ-velocity = -40 km s^{-1} (see Table 8)

is close to the empirical relation found by McLaughlin (1960) from the principal spectra of well observed novae:

$$\log v = 3.7 - 0.5 \log t_3. \quad (14)$$

The small difference between (10) and (11) can be easily understood as a result of non-uniform motion of the envelope caused by the different physical processes. The main important conclusion found from this crude approach is that any expanding component of the main envelope must have a true velocity in the interval between 800 and 1100 km s^{-1}. These values are lower and upper limit of the expansion of the inner envelope, which through measured angular radius give the important restrictions on the distance of the nova. If we suppose uniform expansion with angular rate of 0.293 mas/day and velocities mentioned above, the range of possible distances of Nova V 1974 Cyg is between 1577 and 2168 pc.

6.4. Inner main envelope - detailed model of expansion

As we have shown in chapters 3 and 4, the basic components of the main inner envelope are an equatorial ring and two polar blobs. Radial velocities of emission peaks in the nebular stage of Nova V 1974 Cyg which correspond to the expanding equatorial ring and polar blobs are given in Table 8. Mean radial velocities calculated from receding and approaching components are depicted in Fig. 16.

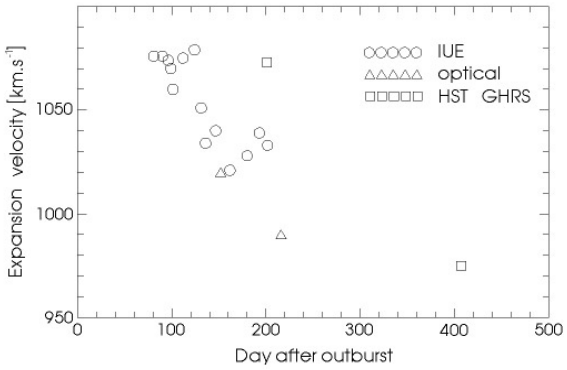

Fig. 14. Expansion velocity of the envelope given by FWHM/2

We can use these data for the calculation of the inclination angle. The basic problem is that the HST data for determination of the expansion rates of the ring and blobs were taken between days 689 and 818, while suitable RV data were obtained between days 79 and 218. Moreover, the ring advances and the inclination angle of the ring changes. If we suppose that the blobs are perpendicular to the ring plane we can use the formulae (4) - (6)

Table 8. Radial velocities of the peaks of nebular emission lines

Reference	Day after outburst	RV^{-}_{ring} [km s^{-1}]	RV^{+}_{ring} [km s^{-1}]	$\overline{RV}_{ring}$ [km s^{-1}]	RV^{-}_{blob} [km s^{-1}]	RV^{+}_{blob} [km s^{-1}]	$\overline{RV}_{blob}$ [km s^{-1}]	$\overline{RV}_{ring}/\overline{RV}_{blob}$	Sp. lines used for RV determ.
Zhang et al. (1992)	79	-585	325	455					H_α
Austin et al. (1996)	217.8			480			860	0.558	H_β, [Ne III]
	318.6			480			860	0.558	[Fe VII]
	413.0			467			798	0.585	H_β, [Ne III], [Fe VII]
	479.9			455			777	0.586	H_β, [Ne III], [Fe VII]
Shore et al. (1993)	201	-554	396	475	-924	789	865.5	0.602	UV: N IV], He II, C III]
	407	-527	432	479.5	-866	783	824.5	0.582	UV: N IV], He II, C III], [Ne IV], [Ne V]
Rafanelli et al. (1995)	519			423					H_α
this paper (optical data)	152	-498	425	461.5	-869	836	852.5	0.541	H_β, [O III]
	216	-536	409	472.5	-919	784	851.5	0.555	H_β, [O III]
	970,971	-541	438	489.5	-883		843	0.581	H_α
	1206	-571	430	500.5					H_α
this paper (UV IUE data)	80.9	-475	420	447.5	-885	741	813	0.550	C III], N III]
	90.2	-467	435	451	-862	776	819	0.551	C III], N III]
	96.2	-475	435	455	-892	783	837.5	0.543	C III], N III]
	98.9	-482	431	456.5	-892	783	837.5	0.545	C III], N III]
	98.9	-482	424	453	-888	765	826.5	0.548	C III], N III]
	101.2	-475	408	441.5	-866	768	817	0.540	C III], N III]
	101.3	-475	395	435	-873	776	824.5	0.528	C III], N III]
	111.8	-482	435	458.5	-881	783	832	0.551	C III], N III]
	124.0	-505	428	466.5	-866	810	838	0.557	C III], N III]
	124.1	-482	438	460	-892	783	837.5	0.549	C III], N III]
	131.1	-482	442	462	-885	806	845	0.547	C III], N III]
	131.2	-497	428	462.5	-870	833	851.5	0.543	C III], N III]
	135.8	-490	428	459	-908	822	865	0.531	C III], N III]
	135.9	-497	443	470	-866	828	847	0.555	C III], N III]
	146.7	-505	454	479.5	-892	787	839.5	0.571	C III], N III]
	161.7	-497	443	470	-889	791	840.5	0.559	C III], N III]
	180.0	-490	450	470	-881	835	858	0.548	C III], N III]
	192.8	-490	442	466	-877	832	854	0.546	C III], N III]
	193.0	-497	443	470	-881	831	856.5	0.549	C III], N III]
	201.6	-505	428	466.5	-907	824	865.5	0.539	C III], N III]
Mean value								**0.554** $\pm$ **0.003**	

$\gamma -$ velocity $= \frac{RV^{-}_{r,b}+RV_{r,b}}{2} = -40 \pm 3 \mathrm{km\,s^{-1}}$

valid for axially symmetric case. The ratio of TV_{blob}/TV_{ring} is equal to ratio of expansion rates for the blobs and the ring given in Fig. 7. The mean ratio of radial velocities of ring and blobs is given in Table 8. The calculated inclination angle of ring and blobs is $i = 35\overset{\circ}{.}1$. This value is in small disagreement both with the mean value of inclination angle of the ring during days 79 and 218 $i' = 30\overset{\circ}{.}9 \pm 1\overset{\circ}{.}1$ found from Fig. 9 and with the inclination angle of the polar outflow $i = 39\overset{\circ}{.}2$ found from the outer envelope. If the inclination angles of the ring i' and the polar axis i differ, we have to use the relation (9) valid for the non-axially symmetric case. If we suppose that $i' = 30\overset{\circ}{.}9$ then $i = 38\overset{\circ}{.}2 \pm 1\overset{\circ}{.}1$ in good agreement with the value of i found from the outer envelope.

6.5. True expansion velocities and history of the expanding shell

The knowledge of the inclination angle i is pivotal for the determination of the true expansion velocities of various parts of both envelopes and the wind at any time after outburst. The un-

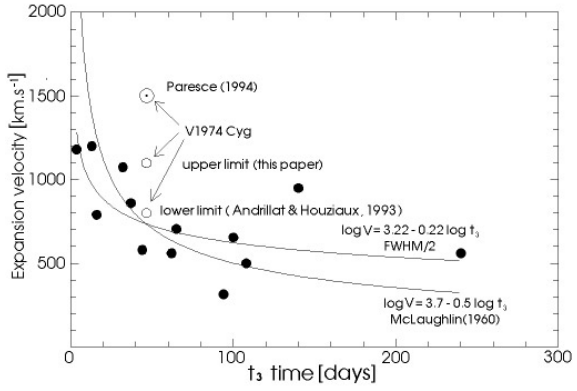

Fig. 15. Expansion velocity of the envelope versus t_3 time relation for 13 well observed novae

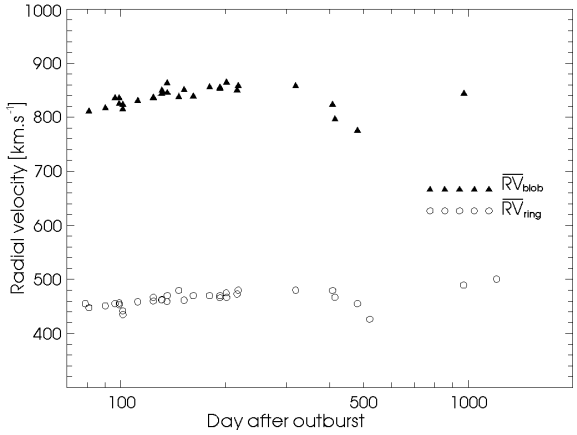

Fig. 16. Mean radial velocities of the ring and blob of expanding massive inner envelope.

weighted mean of both determinations found from the outer and inner envelope is:

$$\mathbf{i = 38^\circ.7 \pm 2^\circ.1.}$$

True expansion velocities of the polar wind and polar outflow of the outer envelope calculated using this value are shown in Fig. 17. True velocities of the spherical wind and the spherical outer envelope are equal to radial velocities of these structures. Terminal velocities of the polar and spherical components of the wind are higher for about 600 km s^{-1} and 1500 km s^{-1}, respectively. A spherical wind increased the velocity from 2200 km s^{-1} on day 5 to about 3000 km s^{-1} on day 50. A polar wind increased the velocity from 5000 km s^{-1} to 6000 km s^{-1} in the same time. The spherical component of the outer low-mass envelope started expansion with an initial velocity of 800 km s^{-1} and through an acceleration by the hot stellar wind reached a velocity of 1700 km s^{-1} on day 45. The polar component of the outer envelope increased the expansion velocity from 1700 km s^{-1} to 3650 km s^{-1} in the same time.

The inner envelope is more complicated than the outer one. It consists of a dense equatorial ring immersed in the spherical lower density envelope, and polar blobs. The polar axis of the blobs is not perpendicular to the equatorial ring plane. Moreover,

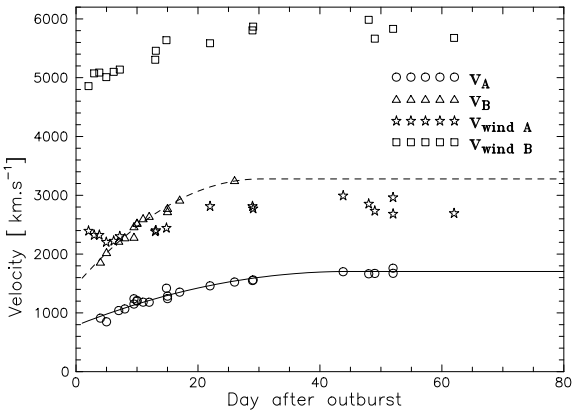

Fig. 17. True expansion velocities of the components of the outer envelope and winds. The dashed line after day 26 was obtained supposing that RV_A /RV_B = 0.596 (see Table 7).

there are indications that the polar axis and equatorial ring plane change the position in space with time.

True expansion velocities of the ring and blobs of the inner envelope are shown in Fig. 18. For the calculation of the true velocities of the ring at any time after the outburst we had to incorporate the observed increase of *i'*. The true expansion velocity of the ring was calculated for every value of RV using the relation (7) and the corresponding value of *i'* given by relation in Fig. 9. The decrease of RV_{blob} with time after day 318 suggests either a true decrease due to interaction with surrounding circumstellar matter and/or an apparent decrease caused by the change of the inclination angle of the blob with time. As it is possible to see from Fig. 10, the blob is double. The first one expands in the initial direction, the second one is located in the centre of the magnetic fountain. Duplicity of the blob is visible also as a double emission peak, formed by the components of the blob in line profile of [Fe VII] in Fig. 9 of the work of Austin et al. (1996) on day 479.9. Unfortunately we have no data for evaluation of the time dependence of the change of the inclination of the blob. We just know that the mean value of *i* between day 80 and 218 is 38.°7 and that *i* = 51.°0 on day 818, but the error of this value is very uncertain. Due to the lack of data we did not incorporate a possible change of the inclination angle of the blob into the calculation of the true expansion velocities, but we used *i* = 38.°7 for all RV_{blob} data.

The inner part of the expanding envelope was ejected with an initial velocity of about 800 km s^{-1} (expansion found from principal spectrum) and accelerated by the stellar wind to 900 km s^{-1} (ring) and 1100 km s^{-1} (blob) around day 200 (Fig. 18). The reasons, why the true velocities of the ring and blob decreased about 200 km s^{-1} and 100 km s^{-1} after day 318 are discussed in Chapter 7.

The data in Fig. 17 and Fig. 18 can be used to calculate the accelerations of the expanding envelopes, caused by the wind. The maximum accelerations in the first days of expansion calculated for the polar and spherical outflow of the outer envelope are 1.4 m s^{-2} and 0.47 m s^{-2}, respectively. The maximum accelera-

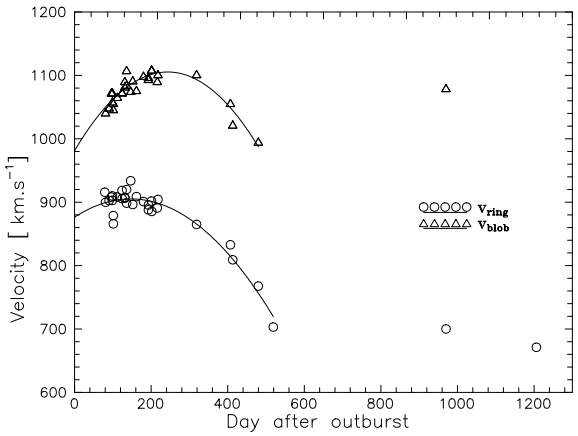

Fig. 18. True expansion velocities of the inner envelope

Table 9. Expansion rates and corresponding distances of the outer envelope (day 172) and the inner envelope (day 480) of Nova V 1974 Cyg.

	Exp. rate [mas/day]	Edge [AU]	Projected edge [AU]	Distance [pc]
Outer envelope				
sphere	0.5523	161	161	1664
polar outflow	0.7558	346	216	1698
Inner envelope				
ring	0.293	240	240	1752
blob	0.214	297	186	1811
Mean value of distance				**1730 ± 30**

tions of the blobs and ring of the inner envelope are 0.012 m s^{-2} and 4.5 10^{-3} m s^{-2}, respectively. Due to the fact that the driving force for acceleration of both envelopes is the same (hot wind), it is clear that the mass of the inner envelope is considerably larger than that of the fast outer envelope. However, the quantitative analysis is highly model-dependent and is beyond the scope of the present paper. The acceleration of the inner envelope of Nova V 1974 Cyg is in agreement with accelerations as found in novae of different speed classes (HR Del, FH Ser, LV Vul) - see Grygar (1981).

6.6. Distance of the nova determined from our kinematic model

Radii of the edges of expanding structures calculated by integrating of parabolic fits through their true velocities are shown in Fig. 19. These data together with expansion rates found from radio and HST images for outer and inner envelope were used for calculation of the distance of the nova.

Bjorkman et al. (1994) showed that the initial mass ejection in Nova V 1974 Cyg was asymmetric and that the degree of asymmetry decreased and then increased in an approximately orthogonal plane during the nebular stage. This result was confirmed by Hjellming (1995), who found from the early radio observations of Nova V 1974 Cyg an outer shell that was expanding in a direction perpendicular to the major axis of the shell observed by HST. Only at later stages the inner shell appeared with the same orientation as the HST image. Explanation of this puzzle is a by-product of our calculation presented above. On day 172 the projection of the edge of the polar outflow of the outer envelope onto the plane perpendicular to the line of sight was still larger than the radius of the sphere. On day 480 the projection of the blob of the inner envelope onto this plane was smaller than the edge of the ring. The larger difference in outflow velocities for components of the outer envelope in comparison with the inner one as well as the inclination of the polar ejecta with respect to the observer can easily explain why the initial mass ejection was asymmetric in one direction, while later on we have observed an expansion in approximately perpendicular direction.

7. Discussion and problems

The most interesting observational fact - decrease of RV velocities of the ring and blobs after day 318 - can be explained either by an interaction of the expanding shell with the circumstellar medium or by other reasons connected with changes of the inclination angle or deviations of the ring from the circular shape.

Following arguments support the first interpretation:

1. Appearance of coronal lines of [Ar X], [Fe X], [Fe XI],[Fe XIV] around day 400 (Austin et al. 1996) with maximum of [Fe X] flux on day 519 (Rafanelli et al. 1995), which could be formed in a hot gas that is heated by interaction of the expanding shell with pre-existing circumstellar gas.

2. An increase of the X-ray flux in the range 0.5-0.9 keV detected on days 434 and 511 (see Fig. 2 of the work Krautter et al. 1996).

If the ejecta from a previous outburst were present, the high velocity wind and outer envelope could interact with them, too. In this case we have to detect hard X-rays when the wind as well as outer envelope reached the remnant material from a former nova outburst or preoutburst outflow. The inner envelope started to meet the circumstellar medium after day 318 at the distance of about 200 AU for blob and 160 AU for ring. Polar and spherical outflows of the outer envelope reached this distance around days 105 and 170, polar and spherical wind on days 56 and 82, respectively. The rise phase of the X-ray light curve was observed from day 63 to 147 and is characterized by a strong continuous increase of the count rate from 0.3 to 11.8 counts s^{-1}. Spectral energy distributions were hard with no counts below 0.8 keV. During the plateau phase, which lasts from day 255 to 511 the counts rates increase to a peak of about 75 counts s^{-1}. Hard energy excess was very weak compared to the soft component. Increase of hard X-ray flux was observed on days 434 and 511. Decline phase observed from day 511 to 653 was characterized by a strong continuum decrease down to 0.2 counts s^{-1}. As it is clearly seen dates of increase of hard X-ray flux are in rough agreement with expected dates of encounters of the components of expanding shell with the circumstellar medium.

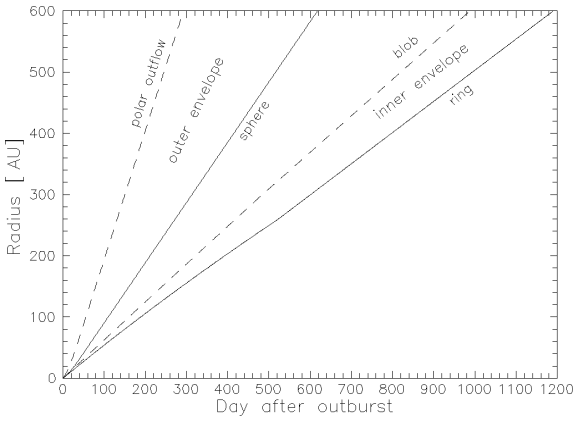

Fig. 19. Radii of the expanding envelopes

The arguments against this interpretation are as follows:

1. Austin et al. (1996) showed that the lines of [Fe VII] 608.7 nm and [Fe X] 647.4 nm can be well fitted by photoionization models, so the expanding gas could be heated by photoionization instead of interaction with circumstellar medium.

2. According to Krautter et al. (1996) the hard X-rays photons detected by the ROSAT satellite arose from the interaction of the expanding nova wind with density condensations within the shell and could not originate at the very outermost parts of the expanding envelope.

In this case the detected decrease of RV of the blob between days 318 and 480 could be explained purely by the change of its inclination angle from 38.7 to 44.7 due to the long time precession of the polar axis and corresponding change in the orientation of the magnetic field. For the ring the situation is more complex. The change of inclination angle included to the data in Fig. 18 does not explain the observed decrease of the velocity. If we reject the interaction with circumstellar medium there exists only one plausible explanation, that there were deviations from circular shape of the ring which have increased with time.

According to Krautter et al. (1996) soft X-rays (0.1 - 0.5 keV) were caused by the radiation of the hot white dwarf remnant on whose surface hydrostatic burning was going on until day 540, when the accreted hydrogen envelope was exhausted. Ivison et al. (1993) proposed from radio observations an instantaneous ejection and a continuous stellar wind as the major driving forces of the gas expansion in Nova V 1974 Cyg. Our results support this interpretation. The wind arising due to the TNR on the surface of white dwarf "snowplows" and accelerates the expanding envelope of Nova V 1974 Cyg. The polar wind could cause the "bar like structure" seen on the first HST image of Nova V 1974 Cyg (Paresce, 1994). Further HST images, which show only an expanding ring, were taken after cessation of the nuclear burning and substantial decrease of the wind density.

Possible existence of the magnetic fountain suggests that the X-rays can be produced by the interaction of light charged particles moving in meridional arcs with the expanding spherical inner lower density envelope. However, quantitative analysis has to be done to reveal the importance of the mechanism for the X-rays production. It is interesting to note that "fountains" or "anemone regions" have been previously found by Tousey et al. (1973) in the EUV observations of the solar active regions. Vourlidas et al. (1996) investigated solar active region NOAA 7124 with the peculiar soft X-ray morphology. Several discrete loops were visible emanating from the region and connecting to the surrounding area, giving it the appearance of a "sea anemone". Anemone regions are usually observed to emerge in magnetic unipolar areas associated with coronal holes. Sometimes they exhibit violent behaviour such as the soft X-ray jets (Shibata et al., 1994).

The orbital period of the underlying binary is 0.08123 days (De Young & Schmidt, 1994). According to Baptista et al. (1993) novae with orbital periods shorter than the period gap appear to be strongly magnetic. The magnetic fountain confirmed the presence of the strong magnetic field in the system. Semeniuk et al. (1995) found another period: 0.085-day, which is continuously decreasing and may be the spin period of the white dwarf component suggesting the presence of an AM Her star which was thrown off synchronism by the nova outburst and now evolves back into synchronization. Retter, Ofek & Leibowitz (1995) reported that the two periods obey exactly the linear relation of Stolz & Schoembs (1981) for SU UMa stars. In this case 0.085-day period is the superhump period and the spin period of white dwarf could be much faster. The very bright old nova V 603 Aql has been classified as a DQ Her type intermediate polar containing a rapidly rotating white dwarf (Schwartzenberg-Czerny, Udalski & Monier, 1992), and as a permanently superhumping extreme SU UMa system (Patterson & Richman, 1991). According to Scott (1995) the existence of an anisotropic wind with a high velocity polar component and prolate ejecta indicates a rapidly rotating white dwarf in the system.

In any case we can conclude that the magnetic field of the white dwarf (which is either a polar or an intermediate polar) play an important role in mass loss from the system and has a large influence in shaping of the nova shell, as well. The magnetic field can also be the cause for the large discrepancy in the rate of decline calculated from t_2 and t_3 time. Mass loss is clearly enhanced by magnetic field effects. Concerning the shaping, there are no doubts that the inner envelope of Nova V 1974 Cyg consists of an equatorial ring and polar blobs. Livio (1994) discussed the importance of the common envelope phase for shaping of nova shells. The mass loss which results from orbital energy deposition occurs preferentially in the orbital plane. Thus a density contrast can be generated between the equatorial (orbital plane) and polar directions. The equatorial ring formed during the common envelope phase expands in the orbital equatorial plane. The coupling of the nova wind and the magnetic field could also shape the nova shell (Orio et al. 1992). According to Chevalier & Luo (1994) the magnetic field in the wind from a magnetized, rotating star becomes increasingly toroidal with distance from the star. Toroidal magnetic tension can constrain the flow in the equatorial region, while not interfering with the flow in polar region. The advance of equatorial ring

Table 10. Rediscussion of the results derived from angular radii of the nova shell

Reference	Day after outburst	Angular radius	radius [AU]	Distance [kpc]	Note
Quirrenbach et al. (1993)	10	0.″002535	5.50	2.17	
Hjellming (1994)	313	0.″175	300	1.71	outer edge of radio shell
		0.″08	162	2.02	inner edge of radio shell
Paresce (1994)	467	0.″13	235	1.80	
Paresce et al. (1995)	467	0.″1387	235	1.69	
Mean value of the distance				**1.88±0.08**	

with time can be caused by complicated common influence of gravitational and magnetic forces on the expanding plasma.

8. True distance of the nova

The discussion of the mechanism of ejection of nova shell has only small influence on the determination of the distance of Nova V 1974 Cygni. In view of the kinematic model presented above we can substantially revise the determination of the distance to the nova as inferred from the angular diameter measurements. The results are summarized in Table 10. The revised distances are remarkably similar and close to the values determined by standard methods (see Table 1).

It should be noted that there exists another rather independent method of the distance determination based on the knowledge of the visual interstellar extinction in the direction of the nova ($l = 89^\circ.5$, $b = +7^\circ.8$). The survey by Neckel & Klare (1980) gives $A_V = 0.56$ mag kpc^{-1} (see also Andrillat & Houziaux 1993). Chochol et al. (1993) determined total $A_V = 0.99$ mag and this leads to the distance $d = 1.77$ kpc, independent of the value of maximum absolute magnitude of the nova.

In conclusion, we are now convinced that the distances of Nova V 1974 Cyg derived by all reliable methods are in excellent mutual agreement (see the mean values in Tables 1, 9, 10 and value mentioned above), amounting to the average $d = (1.77 \pm 0.11)$ kpc in full agreement with the distance of nova published by Chochol et al. (1993).

9. Summary and conclusions

The main results of the present work are the following:

1. The distance of Nova V 1974 Cygni estimated indirectly using MMRD relations is in full agreement with the distance determined directly from the expansion of the envelope leading to the value $d = (1.77 \pm 0.11)$ kpc.

2. Two expanding envelopes were detected - the outer low mass envelope and the inner massive envelope. Both envelopes are prolate.

3. The wind from the white dwarf consists of a spherical and a polar component. The velocity of the polar wind is two times larger than the velocity of the spherical wind. Winds are responsible for shaping of the outer envelope and acceleration of both envelopes.

4. The outer envelope consists of a spherical and a polar component.

5. The inner massive envelope consists of the dense equatorial ring and polar blobs. The ring is immersed in the spherical lower density envelope. The advance of equatorial ring with time was detected.

6. A magnetic fountain that originates in the polar region of the inner envelope was discovered. Interaction of the particles flowing from region of blobs in meridional arcs (flux tubes) with expanding spherical inner envelope is responsible for the origin of observed bright spots detected also as emission knots on high resolution spectra. Shaping of the inner envelope is largely affected by the magnetic field of the white dwarf.

7. The inclination angle of the polar ejecta of both envelopes with respect to the line of sight is $38^\circ.7 \pm 2^\circ.1$.

8. A decrease of expansion velocities of the ring and blob of the inner envelope after day 318 was detected. It can be either caused by the deceleration of the envelope due to the interaction with preoutburst circumstellar shell and/or apparently caused by the change of the inclination angle of the blobs and deviation of the ring from circular shape.

Acknowledgements. We thank to the staff of IUE (M. Barylak) and HST for providing us with the archive data, A. Antalová, S. Balman, J. Gallagher, R. Hjellming, M. Livio, H. Lloyd, T. O'Brien, M. Saniga, A. Skopal, A. Scott for stimulating discussions and M. Bode for reading the manuscript and valuable comments. We express our sincere gratitude to our referee H. W. Duerbeck for his fruitful suggestions, criticism and comments that substantially contributed to the improvement of the paper. The authors are obliged to the referee and to M. Varner for improvements of English. Special thanks belong to Mrs. G. Chocholová for generous financial support and interest in achieved results. This research has been partly supported through the Slovak Academy of Sciences Grant No. 1282/1995.

References

Andrillat Y., Houziaux L., 1993, MNRAS 261, L1
Annuk K., Kolka I., Leedjärv L., 1993, A&A 269, L5
Anupama G.C., Prabhu T.P., 1993, Ann. Israel Phys. Soc. 10, 271
Austin S.J., Starrfield S., Wagner R.M., Shore S.N., Sonnenborn G., 1993, BAAS 25, 833

Austin S.J., Wagner R.M., Starrfield S., Shore S.N., Sonnenborn G., Bertram,R., 1996, AJ 111, 869
Baptista R., Jablonski F.J., Cieslinski D., Steiner J.E., 1993, ApJ 406, L67
Baruffolo A., Rafanelli P., Rosino L., 1992, IAU Circ. No. 5471
Bjorkman K.S., Johansen K.A., Nordsieck K.H., Gallagher J.S., Barger A.J., 1994, ApJ 425, 247
Boyarchuk A.A., Gershberg R.E., 1977 Astron. Zh. 54, 488
Capaccioli M., Della Valle M., D'Onofrio M., Rosino L., 1989, AJ 97, 1622
Capaccioli M., Della Valle M., D'Onofrio M., Rosino L., 1990, ApJ 360, 63
Chevalier R.A., Luo D., 1994, ApJ 421, 225
Chochol D., Hric L., Urban Z., Komžík R., Grygar J., Papoušek J., 1993, A&A 277, 103
Cohen J.G., Rosenthal J., 1983, ApJ 268, 689
Collins P., 1992, IAU Circ. No. 5454
DeYoung J.A., Schmidt R.E., 1994, ApJ 431, L47
Della Valle M., Livio M., 1995, ApJ 452, 704
Elias N.M. et al., 1992, BAAS 24, 1178
Eyres S.P.S., Davis R.J., Bode M.F., 1996, MNRAS 279, 249
Gallagher J.S., Anderson C.M., 1976, ApJ 203, 625
Grygar J., 1981, Scientia 116, 295
Hayward T.L., Gehrz R.D., Miles J.W., Houck J.R., 1992, ApJ 401, L101
Hjellming R.M., 1994, *private communication*
Hjellming R.M., 1995, in A. Bianchini, M. Della Valle and M. Orio (eds.): Cataclysmic Variables, Kluwer, Dordrecht, p. 139
Horn J., 1992, *private communication*
Ivison R.J., Hughes D.H., Lloyd H.M., Bang M.K., Bode M.F., 1993, MNRAS 263, L43
Kolotilov E.A., Nadzhip A.E., Shenavrin V.I., Yudin B.F., 1994, Astron. Reports 38, 548
Krautter J., Ogelman H., Starrfield S., Wichmann R., Pfeffermann E., 1996, ApJ 456, 788
Livio M., 1994, in H. Nussbaumer and A. Orr (eds.): Interacting Binaries, Springer, Berlin, p. 135
Mathis J.S., Cohen D., Finley J.P., Krautter J., 1995, ApJ 449, 320
McLaughlin D.B., 1943, Publ. Obs. Univ. Michigan VIII, No. 12, 149
McLaughlin D.B., 1960, in Stars and Stellar Systems, Vol. 6, J. L. Greenstein (ed.), University of Chicago Press, Chicago, p. 585
Neckel T., Klare G., 1980, A&AS 42, 251
Nota A., Jedrzejewski R., Greenfield, Hack W., 1994, The FOC Instrument Handbook, Version 5.0, ST ScI, Baltimore, MD
Orio M., Trussoni E., Ögelmann H., 1992, A&A 257, 548
Paresce F., 1994, A&A 282, L13
Paresce F., Livio M., Hack W., Korista K., 1995, A&A 299, 823
Patterson J., Richman H., 1991, PASP 103, 735
Pavelin P.E., Davis R.J., Morrison L.V., Bode M.F., Ivison R.J., 1993, Nat 363, 424
Quirrenbach A., Elias N.M., Mozurkewich D., Armstrong J.T., Buscher D.F., Hummel C.A., 1993, AJ 106, 1118
Rafanelli P., Rosino L., Radovich M., 1995, A&A 294, 488
Retter A., Ofek E.O., Leibowitz E.M., 1995, IAU Circ. No. 6158
Schwartzenberg-Czerny A., Udalski A., Monier R., 1992, ApJ 401, L19
Semeniuk I., DeYoung J.A., Pych W., Olech A., Ruszkowski M., Schmidt R.E., 1995, Acta Astron. 45, 365
Scott A.D. 1996, MNRAS (submitted)
Shara M., 1994, AJ 107, 1546
Shibata K., Nitta N., Strong K.T. et al., 1994, ApJ 431, L51
Shore S.N., 1992, BAAS 24, 1256
Shore S.N., Sonneborn G., Starrfield S.G., Gonzales-Riestra R., Ake T.B., 1993, AJ 106, 2408
Shore S.N., Sonneborn G., Starrfield S.G., Gonzales-Riestra R., Polidan R.S., 1994, ApJ 421, 344
Shore S.N., Starrfield S.G., Austin S.J., Gonzales-Riestra R., Sonneborn G., Wagner R.M., 1992, IAU Circ. No. 5523
Slavin A.J., O'Brien T.J., Dunlop J.S., 1995, MNRAS 276, 353
Sparks W.B. et al., 1994, STScI Newsletter 11, No.1, 1
Stolz B., Schoembs R., 1981, IBVS, No. 2029
Tousey R., Bartoe J.-D.F.,Bohlin J.D. et al., 1973, Solar Phys. 33, 269
Vourlidas A., Bastian T.S., Nitta N., Aschwanden M.J., 1996, Solar Phys. 163, 99
Wade R.A., 1990 in A. Cassatella, R. Vioti (eds.): Physics of classical novae, Springer, Berlin p. 122
Zhang X., Zhai D., Guo Y., 1992, Inform. Bull. Variable Stars No. 3783

This article was processed by the author using Springer-Verlag LaTeX A&A style file *L-AA* version 3.